Computers & Geosciences 102 (2017) 45–55

Contents lists available at ScienceDirect

Computers & Geosciences

journal homepage: www.elsevier.com/locate/cageo

Case study

A multi-frequency receiver function inversion approach for crustal velocity structure

Xuelei Li[a,b,c], Zhiwei Li[b,*], Tianyao Hao[a], Sheng Wang[a,c], Jian Xing[a,c]

[a] Key Laboratory of Petroleum Resources Research, Institute of Geology and Geophysics, Chinese Academy of Sciences, Beijing 100029, China
[b] State Key Laboratory of Geodesy and Earth's Dynamics, Institute of Geodesy and Geophysics, Chinese Academy of Sciences, Wuhan 430077, China
[c] University of Chinese Academy of Sciences, Beijing 100049, China

ARTICLE INFO

Keywords:
Receiver function
Multi-frequency
Global optimizing
Crustal velocity structure
Inversion

ABSTRACT

In order to constrain the crustal velocity structures better, we developed a new nonlinear inversion approach based on multi-frequency receiver function waveforms. With the global optimizing algorithm of Differential Evolution (DE), low-frequency receiver function waveforms can primarily constrain large-scale velocity structures, while high-frequency receiver function waveforms show the advantages in recovering small-scale velocity structures. Based on the synthetic tests with multi-frequency receiver function waveforms, the proposed approach can constrain both long- and short-wavelength characteristics of the crustal velocity structures simultaneously. Inversions with real data are also conducted for the seismic stations of KMNB in southeast China and HYB in Indian continent, where crustal structures have been well studied by former researchers. Comparisons of inverted velocity models from previous and our studies suggest good consistency, but better waveform fitness with fewer model parameters are achieved by our proposed approach. Comprehensive tests with synthetic and real data suggest that the proposed inversion approach with multi-frequency receiver function is effective and robust in inverting the crustal velocity structures.

1. Introduction

Teleseismic receiver function waveform contains the P-to-S converted phases generated at subsurface velocity discontinuities and can be derived from teleseismic waveforms by the deconvolution of the vertical component from the horizontal components (Langston, 1979; Owens et al., 1984). The receiver functions have been widely used to estimate the shear velocity structures of the shallow and deep crust, the undulation of the Moho, 410 and 660 km discontinuities (Andrews and Deuss, 2008; Huang et al., 2015; Kosarev et al., 1999; Li et al., 2014, 2016; Vinnik et al., 1983; Zheng et al., 2005; Zhu and Kanamori, 2000). The receiver function waveform inversion has been proven to be effective and reliable to determine the shear wave velocity, Vp/Vs ratio, and crustal thickness as well as the undulation of lithosphere-asthenosphere boundary (LAB) (Borah et al., 2014; Graw et al., 2015; Janiszewski et al., 2013; Julia et al., 2000; Kurose and Yamanaka, 2006; Lawrence et al., 2006; Li et al., 2012, 2013; Mangino et al., 1993; Midzi and Ottemoller, 2001; Yuan et al., 1997). In crustal shear velocity structure studies, most previous inversion algorithms utilized single receiver function waveform with a fixed low-pass frequency. Since receiver function waveforms with different frequencies could include both long- and short-wavelength structures at the same time, it would be a better idea to estimate the crustal velocity structures based on multi-frequency receiver function waveforms. As shown in Fig. 1, the nature of the crust-mantle boundary as a gradational change dominates the large-scale receiver function waveforms at low frequency (e.g. frequency is 0.48 Hz), while a low-velocity zone located in 15–20 km in Fig. 1b results in the small-scale receiver function waveforms at high frequency (e.g. frequency is 1.93 Hz).

Levin et al. (2016) estimated the vertical extent, or sharpness, of the Moho transition based multi-frequency receiver functions, in which the maximum vertical extent was calculated by the highest frequency where the Ps pulse does not lessen. However, the receiver function waveform inversion was not carried out in the study of Levin et al. (2016). Tomfohrde and Nowack (2000) developed a frequency-band inversion method, in which receiver function waveforms with different frequency bands are used to investigate the crustal structure beneath the Taiwan orogen. The method greatly stabilizes the iterative waveform inversion in which the longer wavelength structure can be recovered at lower frequency and then with the upper cutoff frequency increasing, more details would appear (Tomfohrde and Nowack, 2000). Similarly, in order to acquire the trustworthy velocity model, Wu et al.

* Corresponding author.
E-mail address: zwli@whigg.ac.cn (Z. Li).

http://dx.doi.org/10.1016/j.cageo.2017.02.009
Received 16 May 2016; Received in revised form 3 January 2017; Accepted 14 February 2017
Available online 17 February 2017
0098-3004/

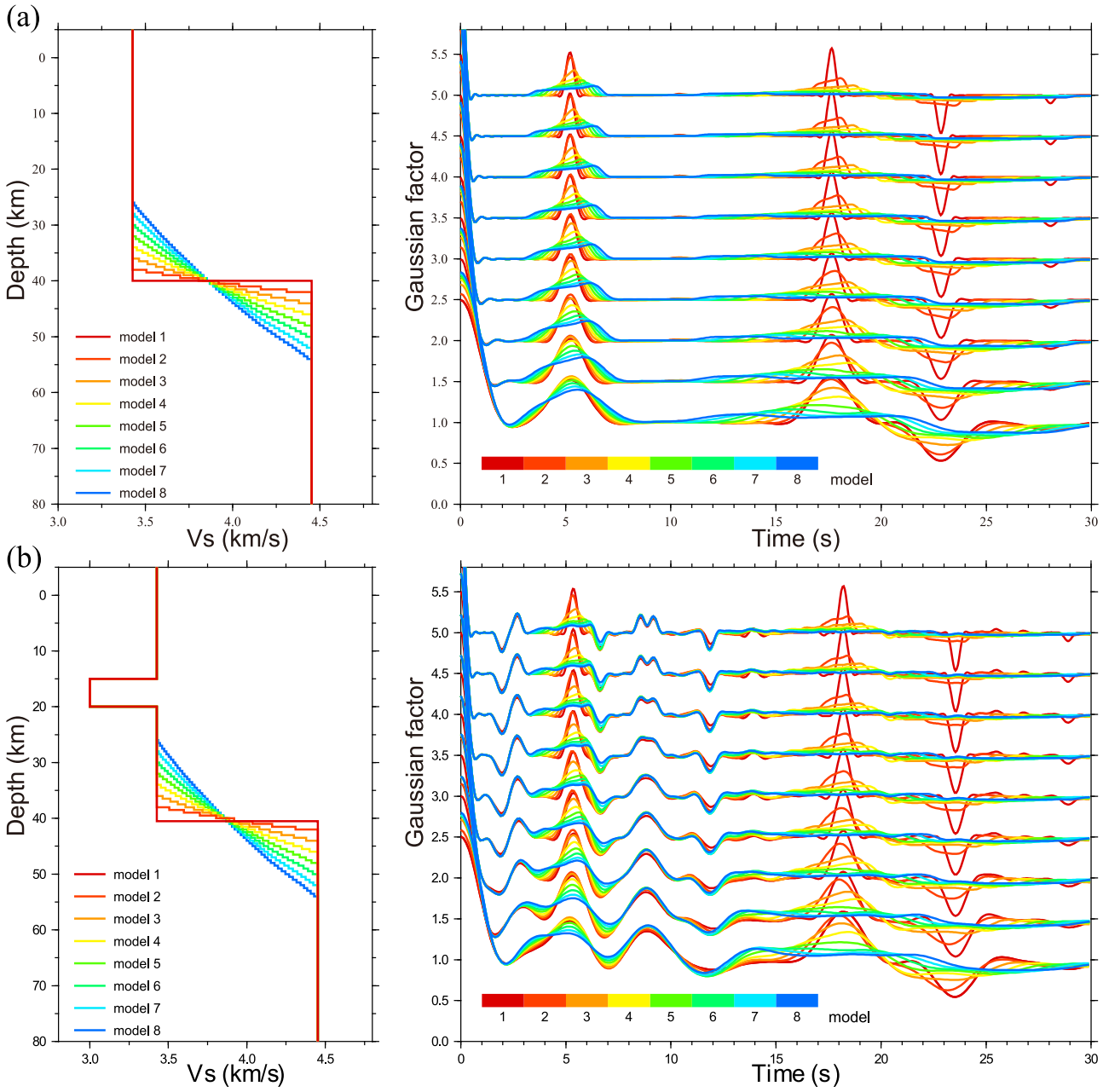

Fig. 1. Receiver functions (right) corresponding to eight velocity structures (left) with different gradational Moho given Gaussian factor of 1.0, 1.5, 2.0, 2.5, 3.0, 3.5, 4.0, 4.5 and 5.0. Along with the increase of Gaussian factor, or cutoff frequency of receiver functions, finer and sharper phase appear in the waveforms. Besides, A low-velocity zone is placed in the crust in (b), which results in complex seismic reverberations in the receiver functions. The incident P wave has a ray parameter of 0.06 s/km, which corresponds to the epicentral distance of 60°.

(2007) decomposed the receiver function waveforms into five resolution scales via Mallat's pyramid algorithm, and then invert the S-wave velocity from the coarsest-scale to finer-scale receiver functions iteratively. The coarsest-scale receiver functions can recover the large-scale velocity model, which is taken as the initial model in the further inversion for finer structures. Receiver functions with finer scale can be used in the inversion to enhance the detailed structure, and the final velocity structure would be obtained after several iterations (Wu et al., 2007).

Although the frequency-band inversions conducted by Tomfohrde and Nowack (2000), as well as the wavelet modeling approach of Wu et al. (2007) can constrain the velocity with different scales, they are conducted by linear inversion. Since the receiver function inversion is known to be highly non-linear and non-uniqueness of its solutions (Ammon et al., 1990), global optimizing techniques such as the DE algorithm, Genetic Algorithms (GA) and Simulated Annealing (SA) have been implemented successfully for receiver function waveform inversion (Li et al., 2010; Shibutani et al., 1996; Vinnik et al., 2004). Differential Evolution (DE) algorithm shows better performance in resolving nonlinear problems (Storn and Price, 1997), and we will apply it to the multi-frequency receiver function inversion to improve computer efficiency.

In this study, our goal is to propose a new tool suitable for receiver function inversions. In the following, we begin with a brief review of receiver function inversion approach. The approach can provide a constraint on the large- and small-scale velocity structures at the same time and achieve the global optimal solution with fewer model parameters (e.g., a small number of layers). Next, synthetic receiver functions are constructed to test the validity of our method. Real receiver functions from the KMNB station in the southeast China and

the HYB station in India are also used to corroborate the proposed approach.

2. Methods

Reflectivity techniques are utilized to compute three-component synthetic receiver functions in a 1-D horizontally stratified isotropic medium (Levin and Park, 1997; Li et al., 2010). The real receiver functions are isolated by the maximum entropy deconvolution method, which has been commonly applied in the isolation of real receiver functions and can achieve high-quality receiver function waveforms (Ai et al., 2003; Wu and Zeng, 1998; Zheng et al., 2005, 2008). A stacking technique is carried out to calculate the average receiver functions, in which the receiver functions are binned at the ray parameter interval of 0.004 s/km. As a result, the moveout correction is not of necessity for this small interval in the receiver function preprocessing. The post-stack reverberations after the first arrival obtained by our stacking technique can be applied in the receiver function inversion, but previous harmonic analysis method of receiver functions of Shen et al. (2013) only uses 10 s waveform information after the first arrival and discards the precious reverberations, which can also be applied to constrain crustal structure.

The flowchart shown in Fig. 2 outlines the data processing and inversion for the proposed approach. The inversion approach is based on the DE algorithm, which has been employed in the earthquake hypocenter location and receiver function waveform inversion (Li et al., 2010; Ruzek and Kvasnicka, 2001). The basic strategy of the DE algorithm can be described as the mutation which generates the different vectors, the crossover which raises the diversity of the perturbed parameter vectors and the selection which determines whether or not a new vector should become a member of the next generation (Storn and Price, 1997). The new population vector possessing the minimum objective function will be retained after all the iterations are finished. This objective function is defined with

$$E(x) = \sum_{i=1}^{M} \frac{w_i n_i}{N} \| O_{ir}(t) - S_{ir}(t) \| \quad (1)$$

where $O_{ir}(t)$ and $S_{ir}(t)$ are real and predicted radial receiver functions of ith bins, respectively; w_i can control the weight in the inversion; n_i is the number of stacked receiver functions with different ray parameters; N is the number of all the receiver functions which is sum of n_i; M is the number of bins about receiver functions equaled to the number of cutoff frequency. The cutoff frequency can be calculated by the Gaussian factor, which is defined by

$$G(w) = e^{-w^2/4a^2} \quad (2)$$

In general, the Gaussian factor parameter, a, is used to quantify the frequency which can be calculated by the given Gaussian factor according to the Eq. (2) if the filter has a value of 0.1. In this study, we select the Gaussian factors of 1.0, 1.5, 2.0, 2.5, 3.0, 3.5 and 4.0 by the trial and error method; their corresponding frequencies are shown in Table 1.

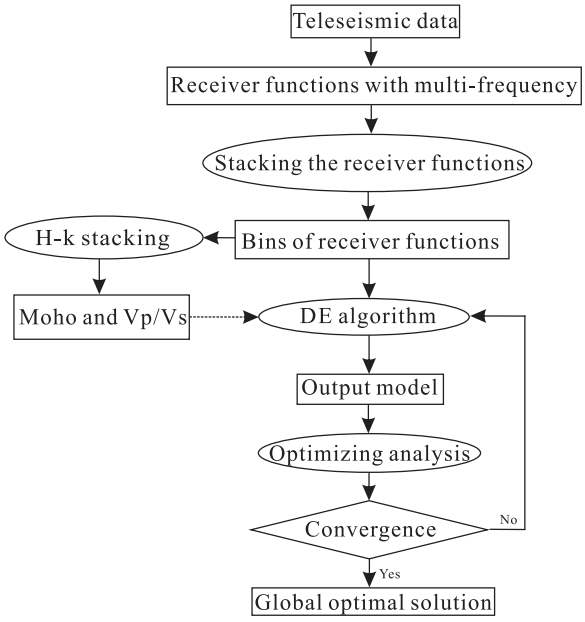

Fig. 2. Flowchart of multi-frequency receiver function waveform inversion with a global optimizing approach.

Table 1
The corresponding relationship among the Gaussian factors, frequency and pulse width.

Gaussian factor	Frequency (Hz) where G (f) =0.1	Approximate Pulse Width (s)
1.0	0.48	1.67
1.5	0.72	1.36
2.0	0.97	1.18
2.5	1.21	1.05
3.0	1.45	0.96
3.5	1.69	0.89
4.0	1.93	0.83

3. Synthetic tests

Three synthetic crustal models are tested to verify the multi-frequency receiver function waveform inversion approach. Synthetic receiver functions with multi-frequency are calculated based on the synthetic models, and the frequencies (controlled by the Gaussian factor) vary from 1.0 to 4.0 at the interval of 0.5. Ray parameters for all the receiver functions are fixed to be 0.06 s/km. The time window of 30 s after the first P arrival is used in the inversion. In this time window, Ps and reverberations between the free surface and Moho are included to constrain the crustal structure effectively. The weighting for different frequencies is set to be the same in the inversion, but it can vary according to the signal-to-noise ratio of the real receiver function waveforms. Besides the noise-free receiver functions, the random noise of 10 per cent of the maximum amplitude of receiver functions is also added to the synthetic receiver functions. Low-pass filters are applied to random noise in order to match dominated frequency of noise to frequency band of receiver functions.

The first test is present by a two-layer model (Fig. 3). The results show that the objective functions (misfit) converge for the synthetic datasets. With random noise datasets, the recovered velocity structure is close to the synthetic model (Fig. 3a and c). The predicted receiver function waveforms with 7 different frequencies maintain the consistency with the synthetic waveforms (Fig. 3b and d). These consistencies of retrieving results over the initial model suggest that our method is effective for the two-layer model.

In order to further verify our approach, a model with five-layer medium is built. As expected, the receiver function waveforms with multiple frequencies have excellent waveform fits between the synthetic and predicted waveforms at either high frequency or low frequency (Fig. 4b and d). In the case of adding random noise, the objective functions still converge and most of the velocity structures are recovered (Fig. 4c and d). The signals caused by a low-velocity zone are clearly revealed at higher frequency, but are almost smoothed out at lower frequency. The results illustrate that the multi-frequency receiver functions are effective for the complex model and can guarantee satisfactory performance for both rough and fine structures simultaneously.

The third test consists of three inversion strategies for the same model with a thin low-velocity zone located between 15 and 18 km in

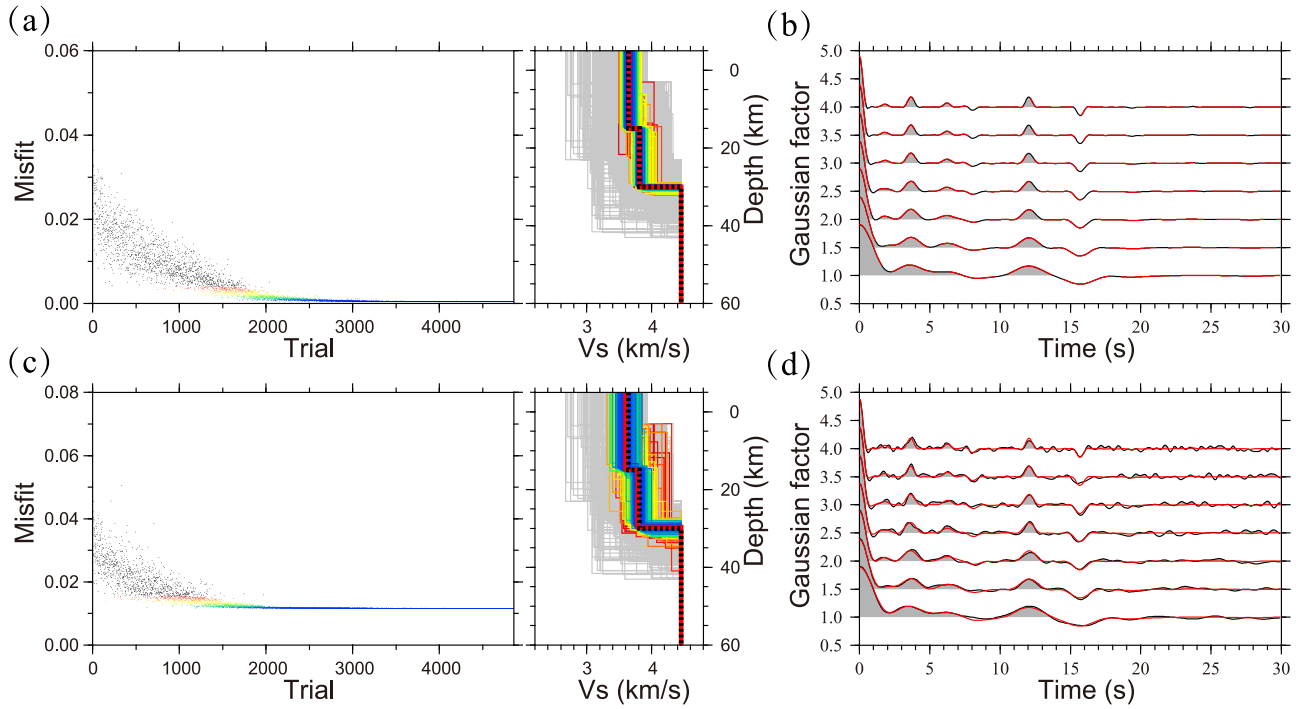

Fig. 3. (a) Inversion results using noise-free receiver functions of 7 different frequency for the two-layer model. Left panels show the decrease of objective functions as the increase of trial. Right panels indicate the true (bold dashed black line) and inversed (bold red line) S-wave velocity model for noise-free data. (b) Receiver functions waveforms for 7 different frequencies corresponding to (a). Black lines and red lines represent the true and inverted receiver function waveforms, respectively. (c) Similar figure to (a) but with 10 per cent noise of the maximum amplitude of receiver functions. (d) Receiver functions waveform corresponding to (c).

the crust (Fig. 5). In the inversions, we focus on two inversion algorithms, multi-frequency receiver function inversion based on the DE algorithm and classic least-square linearized inversion method. Two inversion strategies for traditional least-square method are applied: Iteration inversion from low-frequency to high-frequency and simultaneous inversion with multi-frequency receiver functions. The waveform fits of receiver functions is excellent between the classical least-square linearized inversion method with two strategies and our method from Fig. 5. However, some differences of the velocity structures recovered by three inversion strategies can be identified distinctly. The DE algorithm uses fewer parameters without the initial model and its result is more similar to the real model than other two inversion strategies.

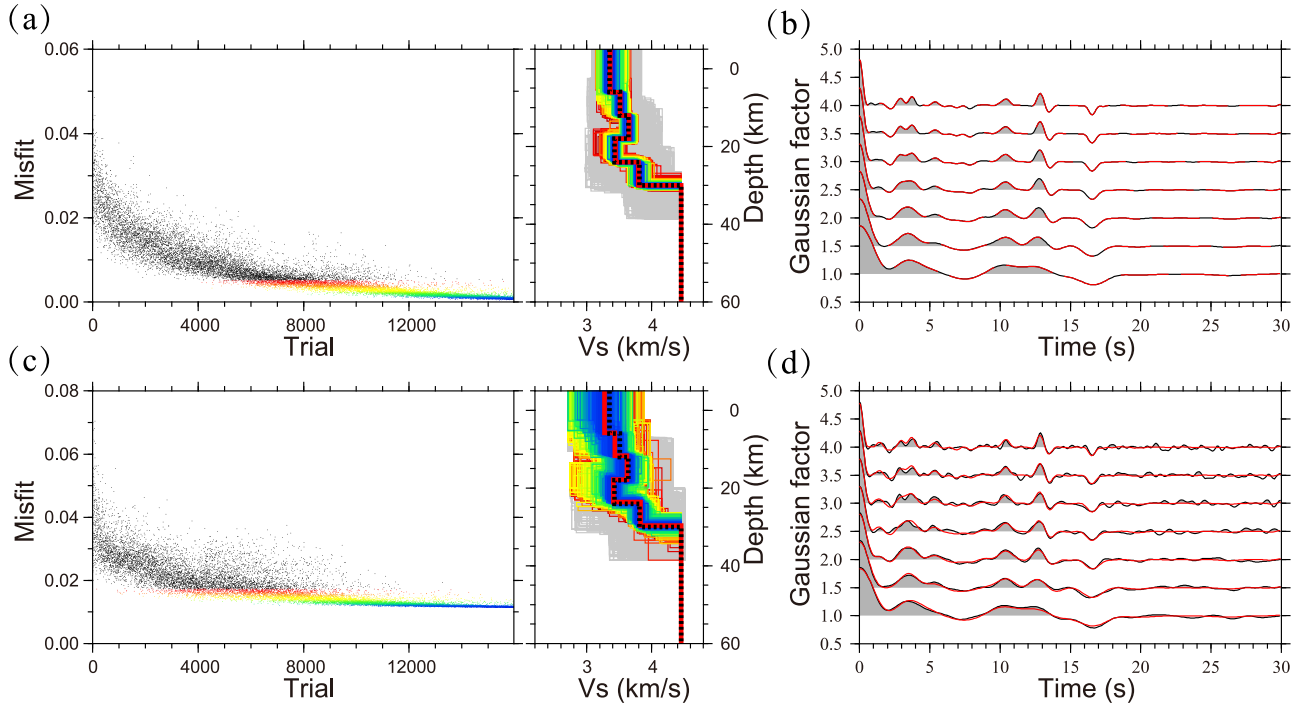

Fig. 4. Similar figure to Fig. 3 but for the five-layer model.

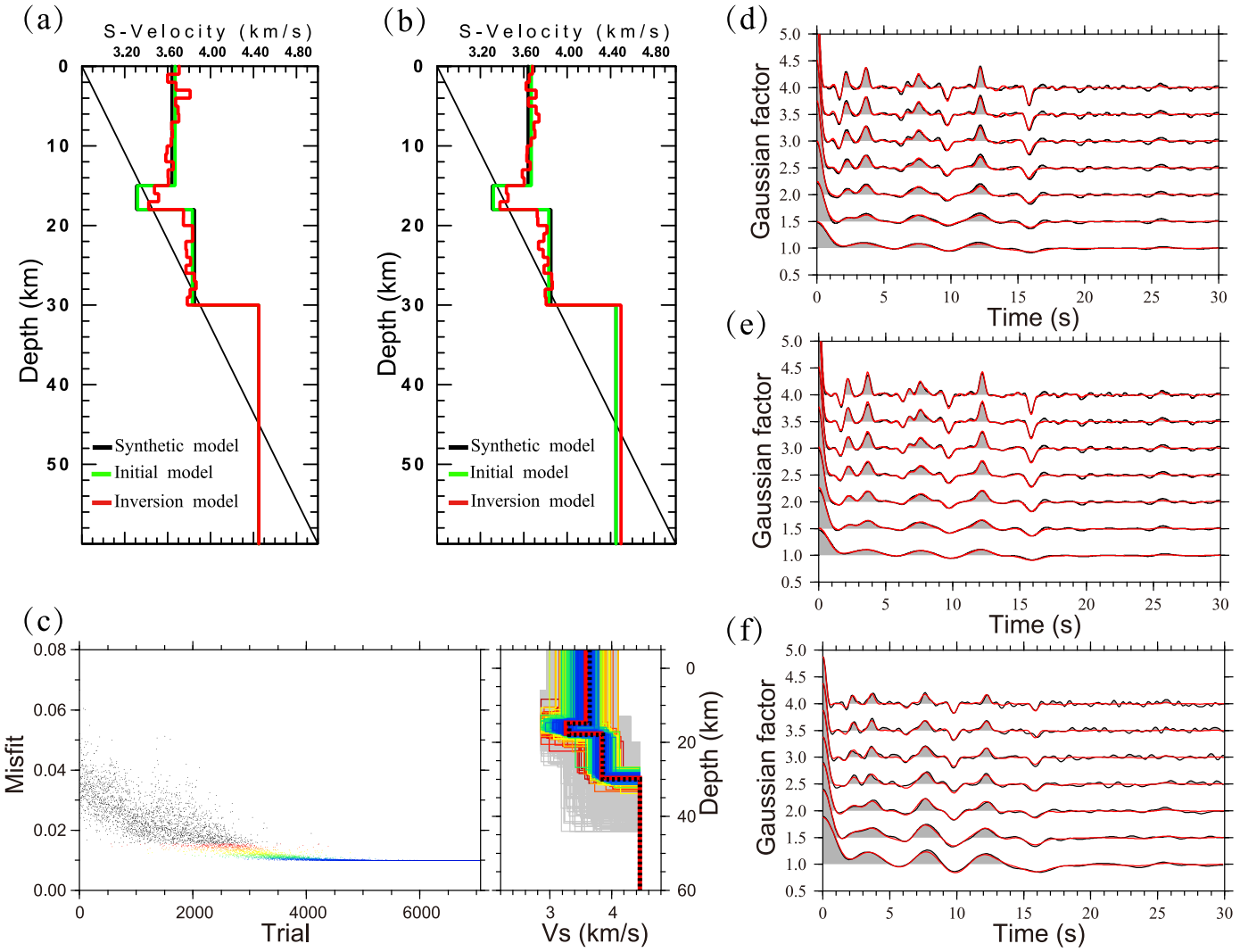

Fig. 5. (a) The iterative inversion result using the linearized least-square method from low to high frequency. (b) The inversion results using linearized least-square method by different frequency. (c) The inversion results by multi-frequency receiver functions with the global optimizing approach of the DE algorithm. (d)–(f) correspond to the receiver functions of (a)–(c), respectively. In linearized inversion, the damping factor, smoothing factor and number of iterations are 1.0, 1.0 and 5, respectively.

4. Real data tests

In this section, the multi-frequency receiver function inversion approach with a global optimizing method is applied to real data from KMNB and HYB stations, which are located in the southeast of China and Hyderabad, India, respectively. Previous studies have indicated a simple crustal structure beneath two stations (Chong et al., 2016; Julia et al., 2009; Kim et al., 2004; Kiselev et al., 2008; Sarkar et al., 2003; Zhou et al., 2000), which contribute to the validation of our results. We select 80 and 220 teleseismic events in the distance range between 30° and 90° for earthquakes with magnitude greater than or equal to 5.5 for KMNB and HYB stations, respectively (Fig. 6a and b). We choose the radial receiver functions with the Gaussian factor of 1.0, 1.5, 2.0, 2.5, 3.0, 3.5 and 4.0, respectively. Then the receiver functions are stacked into a few bins by the ray parameter interval of 0.004 s/km (Fig. 6c–f). This stacking technique conspicuously improves the signal-noise radio of receiver functions and employs a longer waveform window of receiver functions other than harmonic analysis of receiver functions of Shen et al. (2013). This harmonic analysis method of receiver functions only uses 10 s waveform information after the first arrival and discards the precious reverberations, which can also constrain crustal structure (Shen et al., 2013). Meanwhile, $H-\kappa$ stacking method of Zhu and Kanamori (2000) is applied to achieve the Moho depth and average *Vp*/*Vs* ratio of the crustal structure (Fig. 7).

The inversion results are shown in Figs. 8–11. A window of 20 s after the first arrival is used in the inversion, in which contains most phases within the crust according to the real waveform records. As anticipated, the inversion results show that the crustal structure is relatively simple for KMNB and HYB stations, which is consistent with previous results (Fig. 8). Receiver function waveforms fit well for Ps phase, as well as reverberations, including PpPs, PpSs and PsPs phases (Figs. 9 and 10). The waveforms vary from smooth to sharp ones with frequency increased.

In order to verify the results at the KMMB station, the comparisons of velocity structures are performed among ours, CRUST1.0, and the model obtained by Kim et al. (2004) (Fig. 11a). Based on CRUST1.0 and Kim's models, we calculated the corresponding synthetic receiver functions. The misfits between the synthetic and real receiver functions corresponding to different cutoff frequencies are sketched in Fig. 11c. The results suggest that the model produced by our new approach is the best among the models from previous studies.

For the HYB station, the comparison of 7 models including our study, CRUST1.0 and others is present (Fig. 11b). Comparing with the velocity structures from previous studies, the recovered velocity models have better fitness on the observed waveform data (Fig. 11d). Also, the misfits of receiver function waveform gradually decrease with the

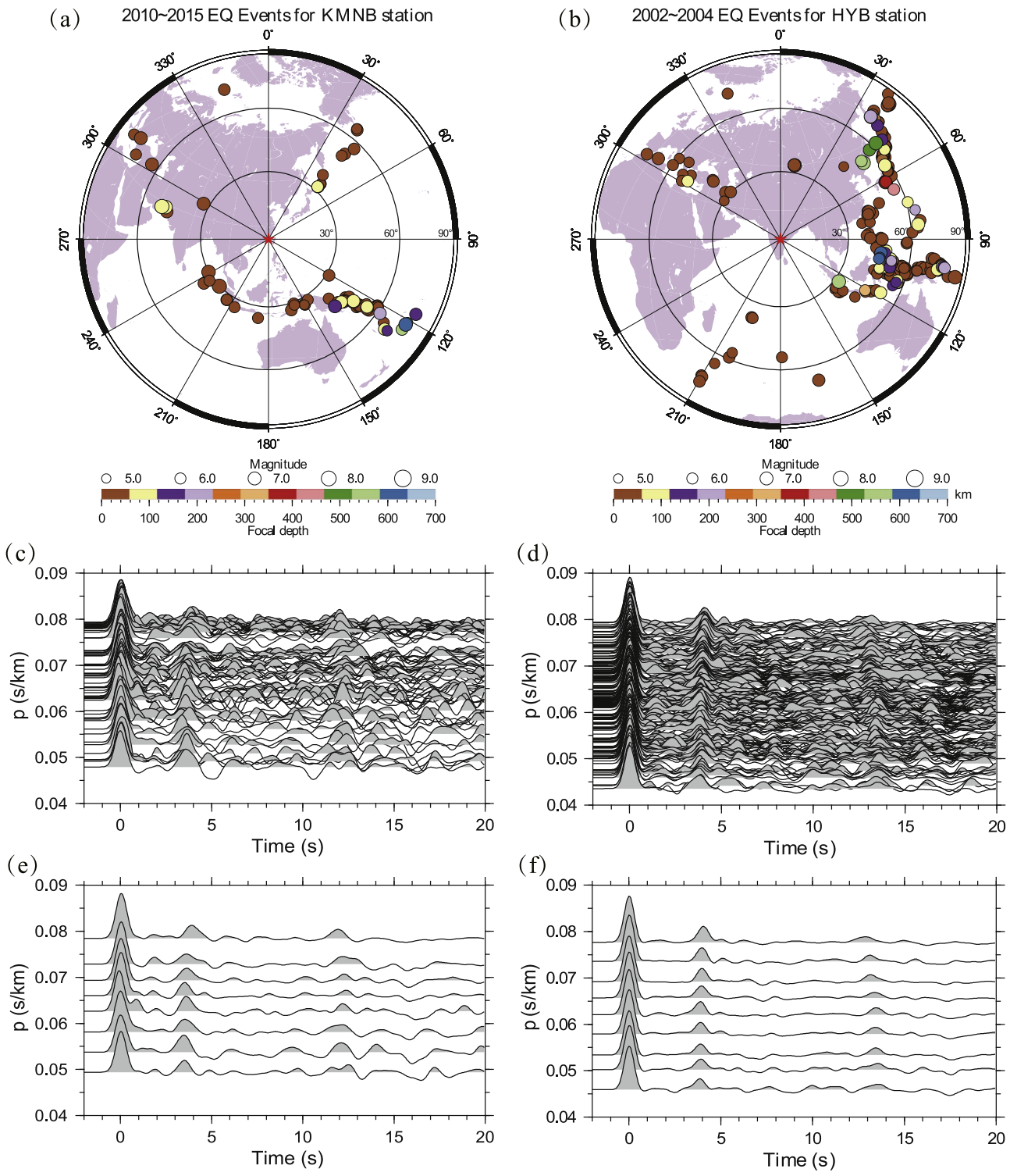

Fig. 6. Epicentral distribution of teleseismic events for receiver functions and two examples of receiver functions stacking. (a), (c) and (e) The KMNB station is located in the southeast China. (b), (d) and (f) The HYB station is located in Hyderabad, India. The pre-stack (c and d) and post-stack (e and f) receiver functions for Gaussian factor of 2.5.

increasing Gaussian factor. Considering the difference of initial data, methods of calculating objective functions, and noise level of real receiver functions, the misfits of these results just provide us with a reference. Nevertheless, these results still demonstrate the effectiveness and reliability of our method. Moreover, we prescribe fewer values of model parameters (e.g. fewer layers) to obtain most of model information in our tests.

5. Discussion

Synthetic and real data tests illustrate that multi-frequency receiver function inversion developed in this study is effective and reliable. The remarkable virtue of this approach is that it makes full use of receiver functions in different frequency bands to constrain the crustal structure simultaneously. Also, this method with a global optimizing method avoids the dependence on the initial model and recovers the majority information of crustal structure by only a few model parameters.

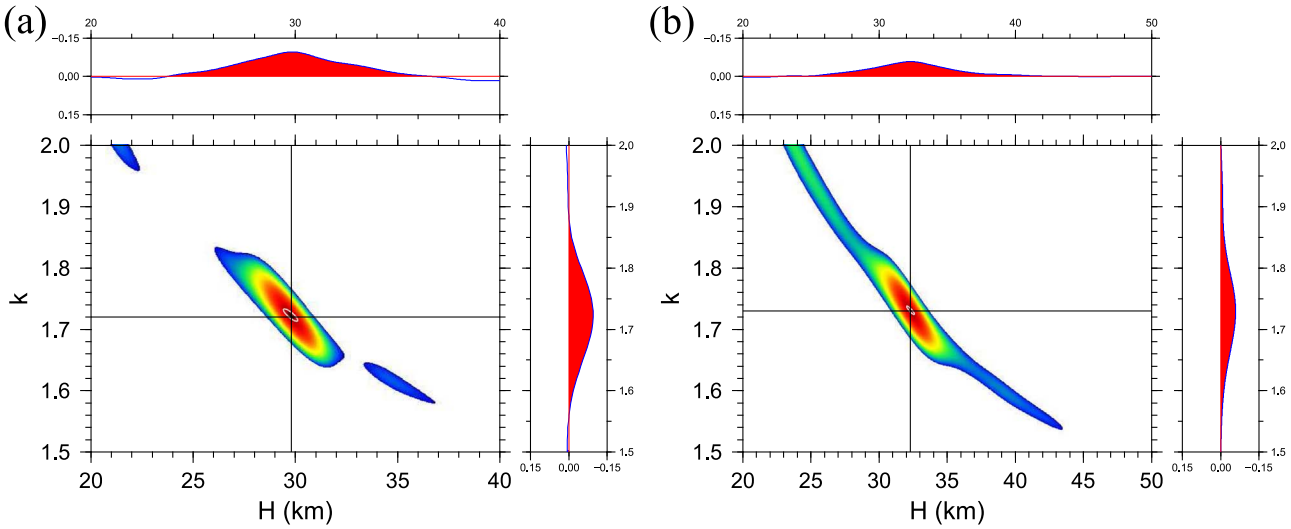

Fig. 7. Results of $H-\kappa$ stacking method for KMNB (a) and HYB (b) stations.

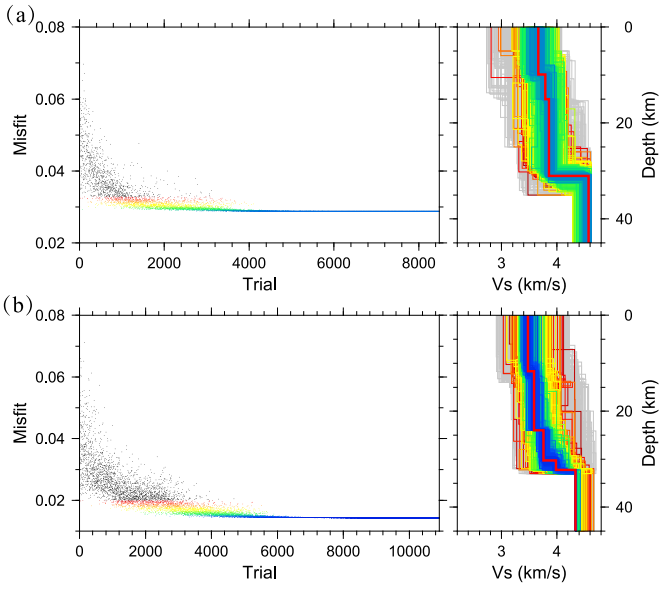

Fig. 8. The results inverted by the multi-frequency receiver functions waveform inversion with a global optimizing approach of the DE algorithm for KMNB (a) and HYB (b) stations.

Comparing with linearized inversion shown in Fig. 5, we found that our method recovered the average velocity structures, which are quite similar to the real model. For two strategies of the least-square linearized inversion method, each layer thickness of the initial model is 1 km. Although the waveforms fitting are good in Fig. 5e and f, the extracted models are not perfect. The inversion leads to a phenomenon of overfitting waveform, which may cause the non-uniqueness of inversion.

The application of our approach to datasets from KMNB and HYB stations confirms the major characteristics beneath the two stations as same as previously obtained in other studies (Chong et al., 2016; Julia et al., 2009; Kim et al., 2004; Kiselev et al., 2008; Sarkar et al., 2003; Zhou et al., 2000). The misfits of our results are smaller than others for KMNB and HYB stations (Fig. 11), but some other details should be mentioned, such as the difference of initial data, methods of calculating objective functions, and noise level of real receiver functions. These factors will give rise to some influence on the misfits calculated.

Although some virtues have been illustrated in our study, several issues about the method are still of necessity to be discussed. We gave a coarse choosing for the Gaussian factor by the trial and error method, and then the Gaussian factor was used to calculate the cutoff frequency with the Eq. (2). As stated in Harland et al. (2009), this excellent selection of Gaussian factor should consider the resolution and high-frequency noise of receiver functions. In our approach, we tuned the Gaussian factor via the trial and error so that we could achieve the Gaussian factor with the minimum misfit. Although we used the same Gaussian factor in the synthetic and real experiments, it could be adjusted according to real problems.

Another controversial problem is the tradeoff between the low and high frequency, especially with the gradational model and low-velocity model. The forward modeling showed that the velocity discontinuity with a gradational change and low-velocity zone cause the change of receiver function waveforms (Fig. 1). According to the results of forward modeling, the gradational model causes the attenuation of different phases, and this attenuation grows with the frequency increasing. Thus, we should apply more low-frequency receiver functions if we want to invert the background velocity structures with the gradation. On the contrary, the reverberations generated by the low velocity zone are remarkable in the high frequency, but smoothed out in the low frequency. As a result, we should use more high-frequency receiver functions if we want to obtain the finer velocity variation with low-velocity zone. In our tests, the equal weight was used for different frequencies. This strategy could obtain the average crustal structure constrained by the multiple frequency receiver functions (e.g. Figs. 3–5). In real receiver function inversion, we can tune the weight of different frequencies to achieve the excellent results.

To summarize, our goal is not to display the excellent results obtained by the proposed approach nor to demonstrate that our approach can outperform other methods in every instance. Instead, our purpose is to describe a new tool suitable for application in receiver function inversion. Our proposed approach still has some flaws in some areas for further improvement. For example, only radial receiver functions were used in the inversion. However, our proposed approach can combine radial and transverse receiver functions in the inversions at the same time, which can be used to constrain the anisotropic structures.

6. Conclusions

We developed an effective and robust receiver function inversion approach with multi-frequency waveform based on a global optimizing method of the DE algorithm. With multi-frequency receiver function waveforms, the proposed approach can effectively constrain on both the long- and short-wavelength characteristics of the crustal velocity

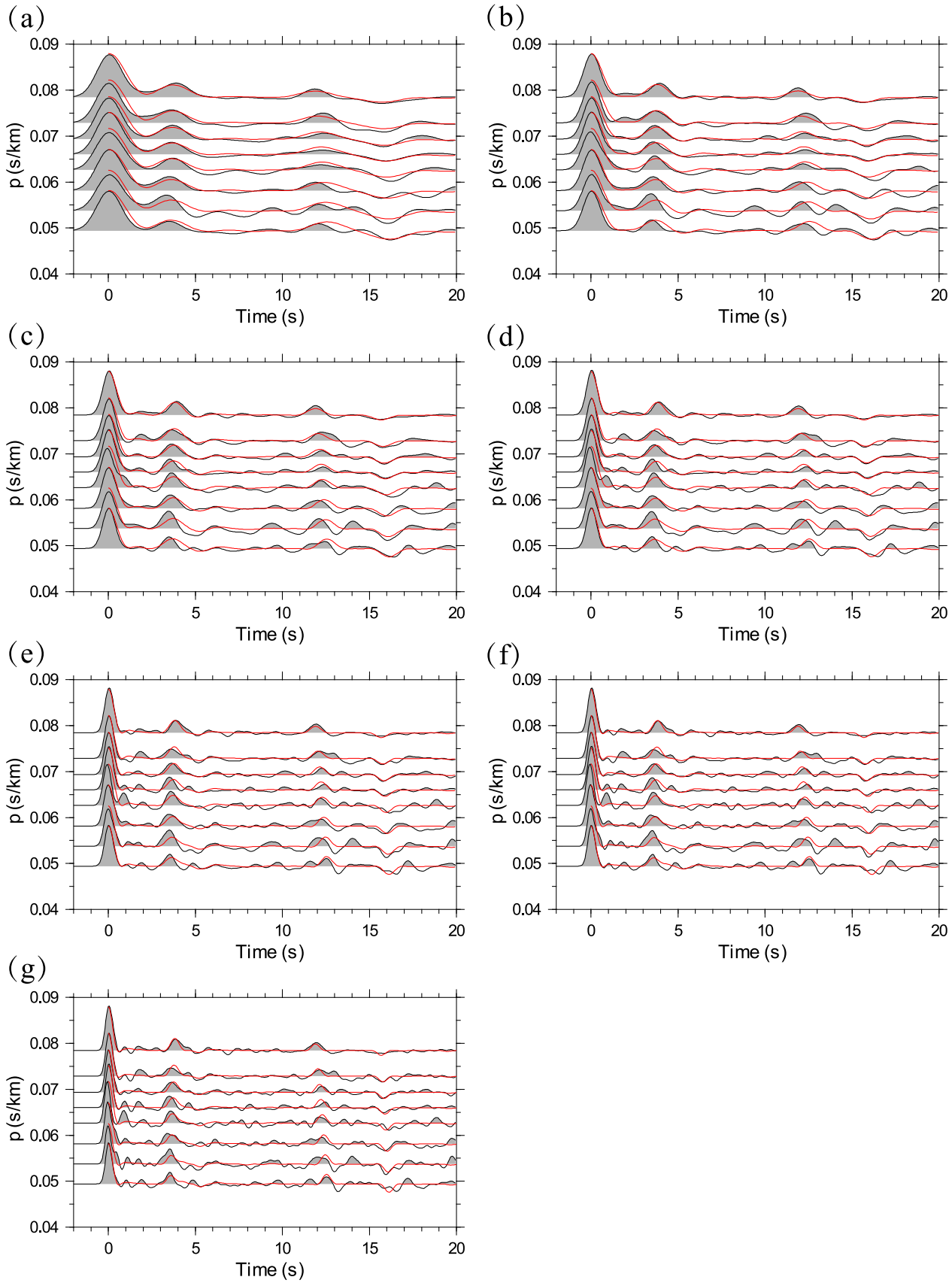

Fig. 9. Waveform fitting between real and synthetic multi-frequency receiver function waveforms at the KMNB station. Gaussian factor has the value of 1.0, 1.5, 2.0, 2.5, 3.0, 3.5, 4.0, 4.5 and 5.0 from (a) to (g). Black and red lines represent the real and synthetic receiver functions, respectively.

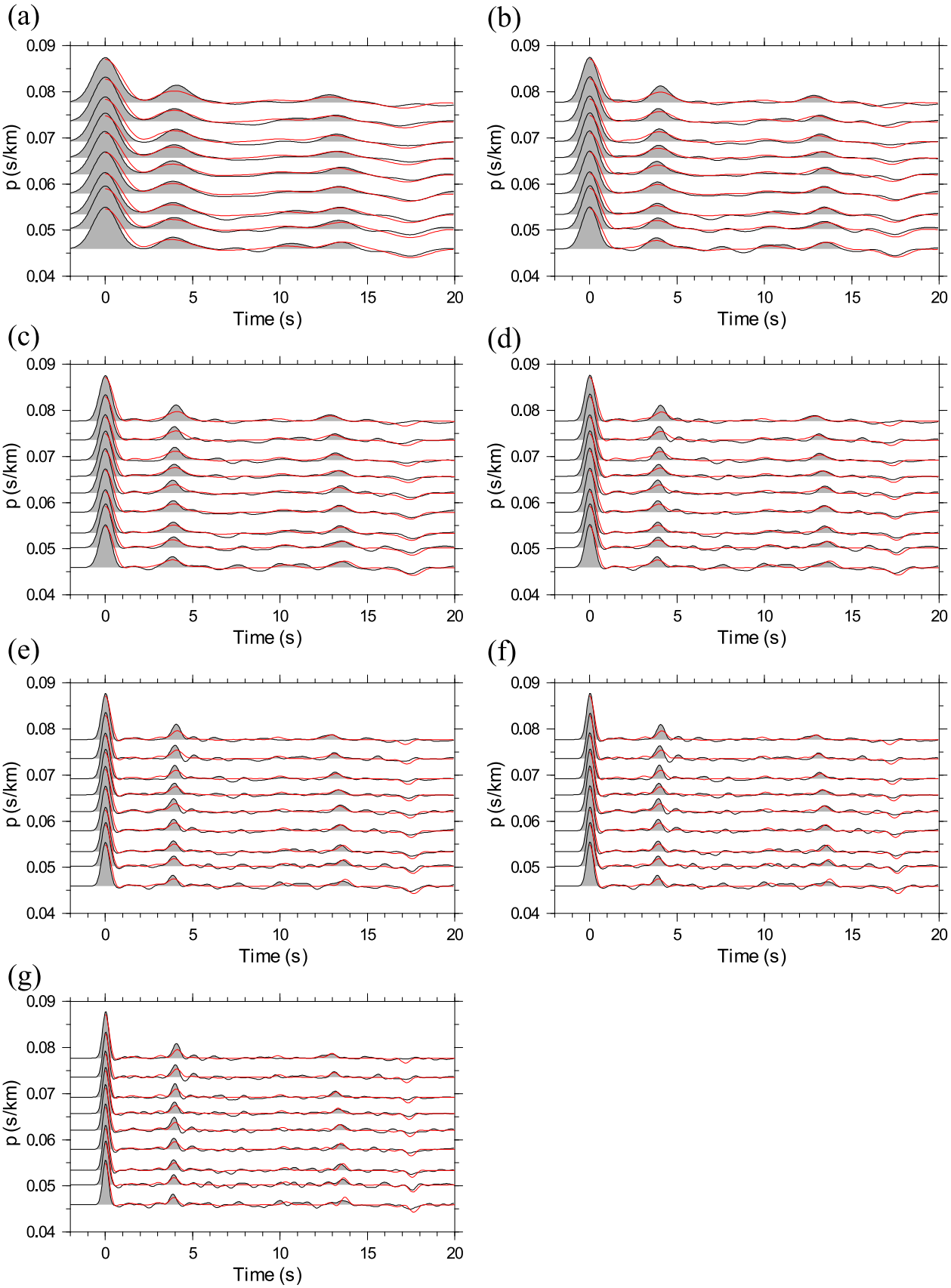

Fig. 10. Waveform fitting between real and synthetic multi-frequency receiver function waveforms at the HYB station. Gaussian factor has the value of 1.0, 1.5, 2.0, 2.5, 3.0, 3.5, 4.0, 4.5 and 5.0 from (a) to (g). Black and red lines represent the real and synthetic receiver functions, respectively.

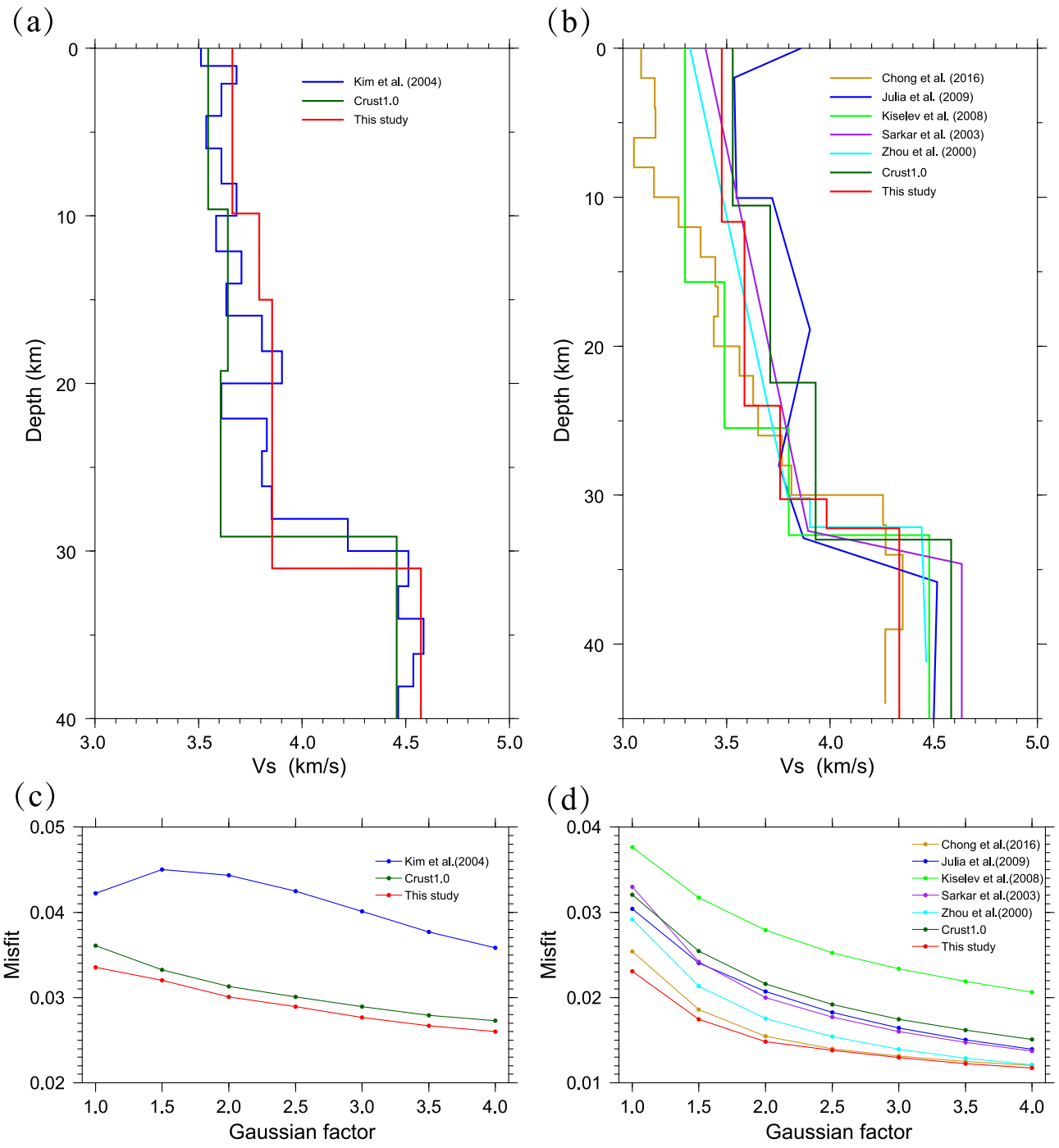

Fig. 11. Crustal model comparisons at KMNB (a) and HYB (b) stations. Misfit between real and synthetic receiver functions from different models at KMNB (c) and HYB (d) stations. Better fitness and reasonably fewer layers are for the models achieved by our proposed approach.

structures at the same time. Crust structures derived from our proposed approach for two seismic stations are consistent with previous results, but show much better fitness on the observed waveforms, suggesting that the multi-frequency receiver function waveform inversion approach can reduce the non-uniqueness in the receiver function inversion, and improve the crustal velocity model. The proposed approach provides a new tool to investigate the crustal structure.

Acknowledgements

Data employed in this study were from the IRIS Data Management Center. We thank the Editor and reviewers for their helpful comments that improve the manuscript. We thank Dr. Jiajun Chong for providing the velocity model beneath HYB station. We are grateful to Professor Sidao Ni and Risheng Chu for helpful comments. This research was supported by GASI-GEOGE-1, NSFC41374139, NSFC41476033, NSFC91428204, NSFC41304045, 2014CB845903, 2013CB733204, XDB06030203 and Youth Innovation Promotion Association CAS.

References

Ai, Y.S., Zheng, T.Y., Xu, W.W., He, Y.M., Dong, D., 2003. A complex 660 km discontinuity beneath northeast China. Earth Planet. Sci. Lett. 212, 63–71.
Ammon, C.J., Randall, G.E., Zandt, G., 1990. On the nonuniqueness of receiver function inversions. J. Geophys. Res. 95, 15303–15318.
Andrews, J., Deuss, A., 2008. Detailed nature of the 660 km region of the mantle from

global receiver function data. Earth Planet. Sci. Lett. 113, B06304.
Borah, K., Rai, S.S., Prakasam, K.S., Gupta, S., Priestley, K., Gaur, V.K., 2014. Seismic imaging of crust beneath the Dharwar Craton, India, from ambient noise and teleseismic receiver function modelling. Geophys. J. Int. 197, 748–767.
Chong, J.J., Ni, S.D., Chu, R.S., Somerville, P., 2016. Joint inversion of body-wave receiver function and Rayleigh-wave ellipticity. Bull. Seismol. Soc. Am. 106, 537–551.
Graw, J.H., Powell, C.A., Langston, C.A., 2015. Crustal and upper mantle velocity structure in the vicinity of the eastern Tennessee seismic zone based upon radial P wave transfer functions. J. Geophys. Res. 120, 243–258.
Harland, K.E., White, R.S., Soosalu, H., 2009. Crustal structure beneath the Faroe Islands from teleseismic receiver functions. Geophys. J. Int. 177, 115–124.
Huang, H.B., Tosi, N., Chang, S.J., Xia, S.H., Qiu, X.L., 2015. Receiver function imaging of the mantle transition zone beneath the South China Block. Geochem. Geophys. Geosystems 16, 3666–3678.
Janiszewski, H.A., Abers, G.A., Shillington, D.J., Calkins, J.A., 2013. Crustal structure along the Aleutian island arc: new insights from receiver functions constrained by active-source data. Geochem. Geophys. Geosystems 14, 2977–2992.
Julia, J., Ammon, C.J., Herrmann, R.B., Correig, A.M., 2000. Joint inversion of receiver function and surface wave dispersion observations. Geophys. J. Int. 143, 99–112.
Julia, J., Jagadeesh, S., Rai, S.S., Owens, T.J., 2009. Deep crustal structure of the Indian shield from joint inversion of P wave receiver functions and Rayleigh wave group velocities: implications for Precambrian crustal evolution. J. Geophys. Res. 114, B10313.
Kim, K.H., Chiu, J.M., Kao, H., Liu, Q.Y., Yeh, Y.H., 2004. A preliminary study of crustal structure in Taiwan region using receiver function analysis. Geophys. J. Int. 159, 146–164.
Kiselev, S., Vinnik, L., Oreshin, S., Gupta, S., Rai, S.S., Singh, A., Kumar, M.R., Mohan, G., 2008. Lithosphere of the Dharwar craton by joint inversion of P and S receiver functions. Geophys. J. Int. 173, 1106–1118.
Kosarev, G., Kind, R., Sobolev, S.V., Yuan, X., Hanka, W., Oreshin, S., 1999. Seismic evidence for a detached Indian lithospheric mantle beneath Tibet. Science 283, 1306–1309.
Kurose, T., Yamanaka, H., 2006. Joint inversion of receiver function and surface-wave phase velocity for estimation of shear-wave velocity of sedimentary layers. Explor. Geophys. 37, 93–101.
Langston, C.A., 1979. Structure under Mount Rainier, Washington, inferred from teleseismic body waves. J. Geophys. Res. 84, 4749–4762.
Lawrence, J.F., Wiens, D.A., Nyblade, A.A., Anandakrishnan, S., Shore, P.J., Voigt, D., 2006. Crust and upper mantle structure of the Transantarctic Mountains and surrounding regions from receiver functions, surface waves, and gravity: implications for uplift models. Geochem. Geophys. Geosystems 7, Q10011.
Levin, V., Park, J., 1997. P-SH conversions in a flat-layered medium with anisotropy of arbitrary orientation. Geophys. J. Int. 131, 253–266.
Levin, V., Tongeren, J., Servali, A., 2016. How sharp is the sharp Archean Moho? Example from eastern Superior Province. Geophys. Res. Lett.. http://dx.doi.org/10.1002/2016GL067729.
Li, Z.W., Hao, T.Y., Xu, Y., Xu, Y., Roecker, S., 2010. A global optimizing approach for waveform inversion of receiver functions. Comput. Geosci. 36, 871–880.
Li, Z.W., Ni, S., Hao, T.Y., Xu, Y., Roecker, S., 2012. Uppermost mantle structure of the eastern margin of the Tibetan plateau from interstation Pn traveltime difference tomography. Earth Planet. Sci. Lett. 335, 195–205.
Li, Z.W., Ni, S.D., Somerville, P., 2014. Resolving shallow shear-wave velocity structure beneath station CBN by Waveform Modeling of the M-w 5.8 Mineral, Virginia, Earthquake Sequence. Bull. Seismol. Soc. Am. 104, 944–952.
Li, Z.W., Ni, S.D., Zhang, B.L., Bao, F., Zhan, S.Q., Deng, Y., Yuen, D.A., 2016. Shallow magma chamber under the Wudalianchi volcanic field unveiled by seismic imaging with dense array. Geophys. Res. Lett. 43, 4954–4961.
Li, Z.W., Tian, B.F., Liu, S., Yang, J.S., 2013. Asperity of the 2013 Lushan earthquake in the eastern margin of Tibetan Plateau from seismic tomography and aftershock relocation. Geophys. J. Int. 195, 2016–2022.
Mangino, S.G., Zandt, G., Ammon, C.J., 1993. The receiver structure beneath Mina, Nevada. Bull. Seismol. Soc. Am. 83, 542–560.
Midzi, V., Ottemoller, L., 2001. Receiver function structure beneath three southern Africa seismic broadband stations. Tectonophysics 339, 443–454.
Owens, T.J., Zandt, G., Taylor, S.R., 1984. Seismic evidence for an ancient rift beneath the Cumberland Plateau, Tennessee – a detailed analysis of broad-band teleseismic p-waveforms. J. Geophys. Res. 89, 7783–7795.
Ruzek, B., Kvasnicka, M., 2001. Differential evolution algorithm in the earthquake hypocenter location. Pure Appl. Geophys. 158, 667–693.
Sarkar, D., Kumar, M.R., Saul, J., Kind, R., Raju, P.S., Chadha, R.K., Shukla, A.K., 2003. A receiver function perspective of the Dharwar craton (India) crustal structure. Geophys. J. Int. 154, 205–211.
Shen, W.S., Ritzwoller, M.H., Schulte-Pelkum, V., Lin, F.C., 2013. Joint inversion of surface wave dispersion and receiver functions: a Bayesian Monte-Carlo approach. Geophys. J. Int. 192, 807–836.
Shibutani, T., Sambridge, M., Kennett, B., 1996. Genetic algorithm inversion for receiver functions with application to crust and uppermost mantle structure beneath eastern Australia. Geophys. Res. Lett. 23, 1829–1832.
Storn, R., Price, K., 1997. Differential evolution – a simple and efficient heuristic for global optimization over continuous spaces. J. Glob. Optim. 11, 341–359.
Tomfohrde, D.A., Nowack, R.L., 2000. Crustal structure beneath Taiwan using frequency-band inversion of receiver function waveforms. Pure Appl. Geophys. 157, 737–764.
Vinnik, L.P., Avetisjan, R.A., Mikhailova, N.G., 1983. Heterogeneities in the Mantle Transition Zone from observations of P-to-Sv converted waves. Phys. Earth Planet. Inter. 33, 149–163.
Vinnik, L.P., Reigber, C., Aleshin, I.M., Kosarev, G.L., Kaban, M.K., Oreshin, S.I., Roecker, S.W., 2004. Receiver function tomography of the central Tien Shan. Earth Planet. Sci. Lett. 225, 131–146.
Wu, Q.J., Li, Y.H., Zhang, R.Q., Zeng, R.S., 2007. Wavelet modelling of broad-band receiver functions. Geophys. J. Int. 170, 534–544.
Wu, Q.J., Zeng, R.S., 1998. The crustal structure of Qinghai–Xizang plateau inferred from broadband teleseismic waveform. Chin. J. Geophys. 41, 669–679.
Yuan, X.H., Ni, J., Kind, R., Mechie, J., Sandvol, E., 1997. Lithospheric and upper mantle structure of southern Tibet from a seismological passive source experiment. J. Geophys. Res. 102, 27491–27500.
Zheng, T.Y., Zhao, L., Chen, L., 2005. A detailed receiver function image of the sedimentary structure in the Bohai Bay Basin. Phys. Earth Planet. Inter. 152, 129–143.
Zheng, T.Y., Zhao, L., Zhu, R.X., 2008. Insight into the geodynamics of cratonic reactivation from seismic analysis of the crust-mantle boundary. Geophys. Res. Lett., 35.
Zhou, L.M., Chen, W.P., Ozalaybey, S., 2000. Seismic properties of the central Indian shield. Bull. Seismol. Soc. Am. 90, 1295–1304.
Zhu, L.P., Kanamori, H., 2000. Moho depth variation in southern California from teleseismic receiver functions. J. Geophys. Res. 105, 2969–2980.